Induced antiferromagnetism in $HoFeO_3$

1995 J. Phys.: Condens. Matter 7 8099

(http://iopscience.iop.org/0953-8984/7/42/007)

J. Phys.: Condens. Matter 7 (1995) 8099–8107. Printed in the UK

Induced antiferromagnetism in $HoFeO_3$

S Bujko†, D Georgiev†, K Krezhov‡, V Nietz† and G Passage‡

† Frank Laboratory of Neutron Physics, Joint Institute of Nuclear Research, 141980 Dubna, Russia

‡ *Institute of Nuclear Research and Nuclear Energy, Bulgarian Academy of Sciences,* 72 Tzarigradsko Chaussee Boulevard, 1784 Sofia, Bulgaria

Received 4 May 1995, in final form 14 August 1995

Abstract. We present results from neutron diffraction studies of single crystalline $HoFeO_3$ in a pulsed magnetic field by means of the spectrometer SNIM-2 at JINR-Dubna. The weak antiferromagnetism induced by the applied field in the Fe^{3+} and Ho^{3+} ion sublattices is measured in the temperature range 79–154 K. The temperature dependence of the antiferromagnetic susceptibility of the holmium subsystem is derived and found to obey the Curie–Weiss law.

1. Introduction

The crystalline symmetry of $HoFeO_3$ is described by the orthorhombic space group D_{2h}^{16}—*Pbnm*. The unit cell contains four formula units and the positions of the magnetic ions Ho^{3+} and Fe^{3+} are depicted schematically in figure 1. The four iron ions are in the parameterless special positions 4(b): $(0, \frac{1}{2}, 0)$ and the four rare-earth ions are in the special positions 4(c): $(x, y, \frac{1}{4})$. This structure allows a non-collinear antiferromagnetic Fe^{3+} spin arrangement with a net weak ferromagnetism present. At temperatures below the first Néel temperature $T_{N1} = 647$ K [1] the Fe sublattices are ordered antiferromagnetically, while the Ho sublattices retain the paramagnetic state down to the liquid helium temperature range. However, with lowering temperature the spins of the holmium ions become increasingly polarized due to the exchange interaction between Ho and Fe, and the character of this polarization is determined in turn by the ordering configuration of iron spins. The long-range magnetic ordering of the holmium sublattices is observed below a Néel temperature reported as $T_{N2} = 4.5$ K [1] and $T_{N2} = 6.5$ K [2].

In accordance with the notation commonly accepted in considering the possible magnetic structures (see e.g. [3]) we use the following vectors of ferromagnetism and antiferromagnetism: $\boldsymbol{F} = \boldsymbol{M}_1 + \boldsymbol{M}_2 + \boldsymbol{M}_3 + \boldsymbol{M}_4$, $\boldsymbol{G} = \boldsymbol{M}_1 - \boldsymbol{M}_2 + \boldsymbol{M}_3 - \boldsymbol{M}_4$, $\boldsymbol{C} = \boldsymbol{M}_1 + \boldsymbol{M}_2 - \boldsymbol{M}_3 - \boldsymbol{M}_4$, $\boldsymbol{A} = \boldsymbol{M}_1 - \boldsymbol{M}_2 - \boldsymbol{M}_3 + \boldsymbol{M}_4$ for the Fe ions and $\boldsymbol{f} = \boldsymbol{M}_5 + \boldsymbol{M}_6 + \boldsymbol{M}_7 + \boldsymbol{M}_8$, $\boldsymbol{g} = \boldsymbol{M}_5 - \boldsymbol{M}_6 + \boldsymbol{M}_7 - \boldsymbol{M}_8$, $\boldsymbol{c} = \boldsymbol{M}_5 + \boldsymbol{M}_6 - \boldsymbol{M}_7 - \boldsymbol{M}_8$, $\boldsymbol{a} = \boldsymbol{M}_5 - \boldsymbol{M}_6 - \boldsymbol{M}_7 + \boldsymbol{M}_8$ for the Ho ions (where $\boldsymbol{M}_i$ denotes the magnetization of the ith sublattice).

In the temperature range $T_2 = 63\,\mathrm{K} < T < T_{N1}$, the magnetic phase Γ_4 ($G_xA_yF_zf_z$) is established, with a basic antiferromagnetic Fe^{3+} spin arrangement of the **G** type along the x axis and small-in-magnitude additional components as given in the parentheses, where x, y, z correspond to a, b, c orthorhombic crystal axes. At temperatures $T < T_1 = 51$ K the magnetic state Γ_2 ($G_zC_yF_xf_xc_y$) is found with the basic antiferromagnetic vector $\boldsymbol{G}$ directed along the z axis (c axis). The temperature-driven magnetic phase transition Γ_4–Γ_2 is of the spin reorientation type. With changing temperature from T_1 to T_2 the vector $\boldsymbol{G}$

0953-8984/95/428099+09$19.50

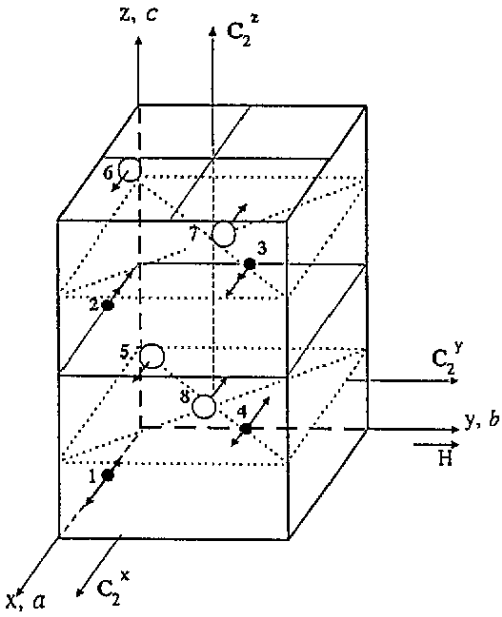

Figure 1. Position of magnetic ions in the unit cell of $HoFeO_3$. The initial moments of Fe^{3+} ions are labelled by longer arrows. Shorter arrows at Fe^{3+} positions and the arrows at Ho^{3+} positions label magnetizations of type **C** and **c** (see text) induced by an external magnetic field.

rotates from the z to the x axis. During the reorientation the vector G remains in the xz plane and all vector constituents of Γ_2 and Γ_4 phases are non-zero.

Under the action of an external magnetic field applied along the y axis, in the temperature region $T_2 < T < T_{N1}$ the main phase Γ_4 becomes mixed with a small induced admixture of the state $\Gamma_3(C_x, F_y, A_z, c_x, f_y)$, i.e. iron and holmium spins are ordered antiferromagnetically of (**C, c**) type along the x axis. The degree of such ordering is proportional to the magnetic field magnitude, and for Fe^{3+} ions it is determined mainly by the antisymmetric exchange Fe–Fe interaction [4], while for Ho^{3+} ions it is the antisymmetric and anisotropic-symmetric exchange Ho–Fe interactions that play a part [5]. Thus, the experimental investigation of antiferromagnetic ordering induced by external magnetic field applied along the y axis, H_y, enables the determination of the corresponding exchange constants, which is of essential importance in research on rare-earth orthoferrites.

However, to separate experimentally the corresponding antiferromagnetic components is not a simple task, because these interactions are some orders of magnitude weaker than the principal exchange interaction responsible for Fe^{3+} ion ordering. This explains the fact that such studies on this matter have not yet been published.

In this respect, neutron diffraction techniques offer unique opportunities because the induced antiferromagnetic components (**C, c**) give rise to the appearance of single diffraction peaks which are not related to other components of the sublattice magnetization or nuclear scattering contributions. It is worth noting, however, that such experiments at stationary reactors will encounter difficulties because of the rather high applied magnetic fields needed.

The pulse reactor IBR-2 at JINR, featuring a combination of a low frequency of repeated bursts of power and associated high-intensity neutron pulses with a source providing a variable-intensity pulse magnetic field, made possible studies of field-induced weak antiferromagnetism. In this paper we present the first results obtained on single crystalline $HoFeO_3$ by means of the spectrometer SNIM-2.

2. Experimental details

The measurements were carried out by means of the neutron spectrometer SNIM-2, which combines the neutron time-of-flight diffraction equipment ND-3 [6] and the pulse magnetic facility IMU-2 [7]. The preliminary oriented single crystal of $HoFeO_3$, with dimensions $3 \times 6 \times 8\,mm^3$, was cemented to the bottom part of the heat exchanger, which is a 100 mm long rod of BeO ceramics, 7 mm in diameter, with its upper end held at liquid helium temperature. The cryostat tail with the glued sample was centred within the magnetic unit, which generates a vertically directed pulse magnetic field. The assembly was then mounted on the table of ND-3 at the exit of the curved mirror neutron guide, so that the neutron flight-path sample-moderator was 30 m. Accurate orientation of the single crystal sample and the transition from one vertical plane to another was achieved by rotating the whole cryostat assembly about the vertical axis. The accessible range of sample temperatures was 30–400 K. The temperature inhomogeneity within the volume of a sample with above specified dimensions was less than 1 K. The temperature was maintained within 1% over the operating region. The neutrons scattered on the specimen studied were collected by a detector mounted on the rotating arm of the diffractometer unit. The sample–detector distance was 2.17 m.

The detector was a cylindrical ^3He neutron counter, 90 mm in diameter and with an in-beam irradiated effective thickness of 10 mm. The counter dimensions ensured the collection of all neutrons undergoing diffraction on the single crystal which were scattered within the covered solid angle.

The shape of magnetic field pulses was of a half-period sine waveform (with a slight attenuation), with a duration of 700 μs in this study. An inductive transducer coupled to the sample was used to measure the magnetic field pulse shape, which was needed in the treatment of data. The inhomogeneity of the axial field component was less than 1% within a specimen of above-mentioned dimensions. The pulse amplitude was maintained at a preset level within 0.5%.

In order to get the absolute magnitudes of the induced components C_x and c_x, it is necessary to know the intensity distribution of the primary neutron beam as a function of neutron wavelength, $i(\lambda)$. This was achieved by prolonged time-of-flight measurements on vanadium placed at the sample position using the same ^3He counter. The spectrum $i(\lambda)$ is obtained from the expression for the scattering intensity on vanadium:

$$I(\lambda) = i(\lambda) 2\sigma_{inc} \frac{V_{van} S_d}{4\pi L^2 a^3} \tag{1}$$

where a is the lattice cell parameter, V_{van} is the sample volume and $\sigma_{inc} = 5.1$ barn is the incoherent scattering cross section of vanadium, S_d is the detector area and L is the distance between the sample and the detector. The incident neutron spectrum is shown in figure 2.

In measuring the changes in crystal reflectivity induced by alternating magnetic field the time resolution becomes of great importance. It is to be taken into account that, due to the finite energy width of the neutrons undergoing diffraction and sensing the information on the sample state, there is a certain admixture of the gained information during the flight time between the scattering event and the registration event. Since crystal mosaicity is substantially lower than the angular divergence of the primary beam, the time resolution can be expressed in the form [8]

$$\delta t = T\sqrt{(\Delta L/L)^2 + (\Delta L/\tan\theta)^2} \tag{2}$$

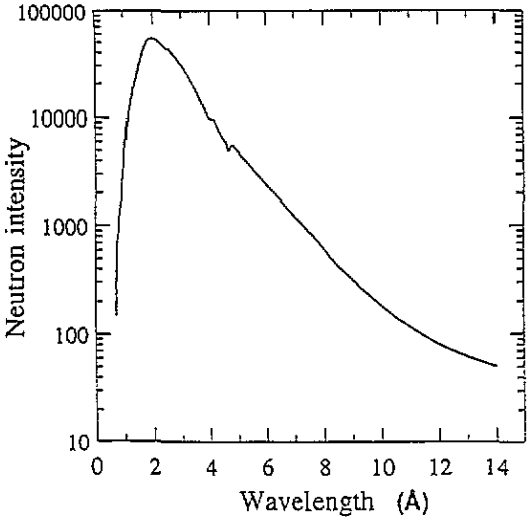

Figure 2. Shape of the primary neutron beam.

where $T = 252.43L\lambda$ is the flight time along the flight path L between the sample and the detector, ΔL is the flight path uncertainty related to the sample size and the effective thickness of the detector, and θ is the Bragg angle. Here δt and T are measured in μs, λ in Å, and L and ΔL are in m. Correspondingly, the resolution with regard to the amplitude of the magnetic field of sine waveform is

$$\frac{\delta H}{H_m} = \frac{\delta t}{T_H}\pi \cos\left(\pi \frac{t}{T_H}\right) \tag{3}$$

where H_m and T_m are the amplitude and duration of the magnetic field pulse. In our study $L = 2.17\,\text{m}$, $\Delta L = 0.01\,\text{m}$, $\Delta\theta = 1.5 \times 10^{-3}\,\text{rad}$, $H_m = 75$–$90\,\text{kOe}$ and $T_H = 700\mu\text{s}$, so that the dependence on neutron wavelength λ of the time resolution δt is 5–$10\,\mu\text{s}$, but usually the channel width of the time analyser exceeds this value. The relative resolution with regard to the field amplitude at the initial part of the pulse is $\delta H/H_m = 2$–4%.

3. Experimental data and their analysis

Two diffraction reflections sensitive to the above-mentioned components of the mixed phase of states Γ_4 and Γ_3 were measured in the present study: (102) associated with components C_x, c_x and (201) associated with components c_x, A_y, A_z.

The component A_y is not zero at $H = 0$. Our recent paper [9] was devoted to its determination; see the earlier work with polarized neutrons [10] as well. In an approximation linear with respect to the magnetic field the component A_y should not change. The component A_z is induced by a field H_y and it can be neglected because, as shown in [5], it appears in the Hamiltonian invariantly related with the component C_x only, i.e. it can be exhibited only in an approximation quadratic with respect to the field, in contrast to the components C_x and c_x which enter the Hamiltonian in combinations of the form C_xF_y and c_xF_y. Thus the measurement of two diffraction reflections gives us the opportunity to determine the magnitude of induced antiferromagnetism along the x axis in the iron and rare-earth subsystems separately.

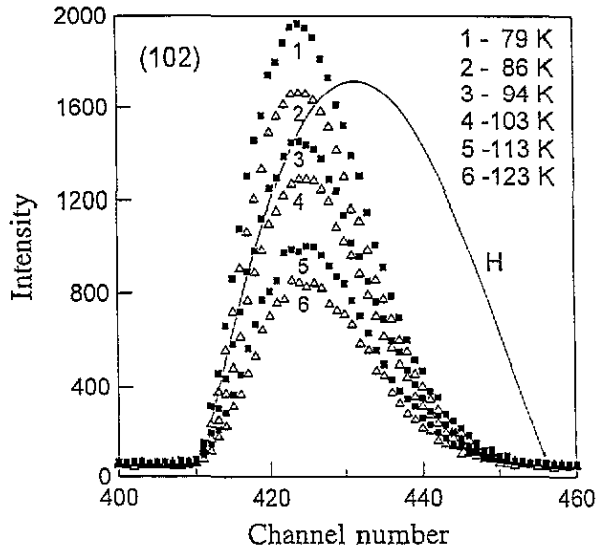

Figure 3. Neutron diffraction profile of (102) reflection at different temperatures in a pulsed magnetic field with amplitude $H_m = 77$ kOe. The magnetic field pulse intensity H against channel number is shown for comparison. The channel width of time analyser is $\tau = 16\,\mu$s.

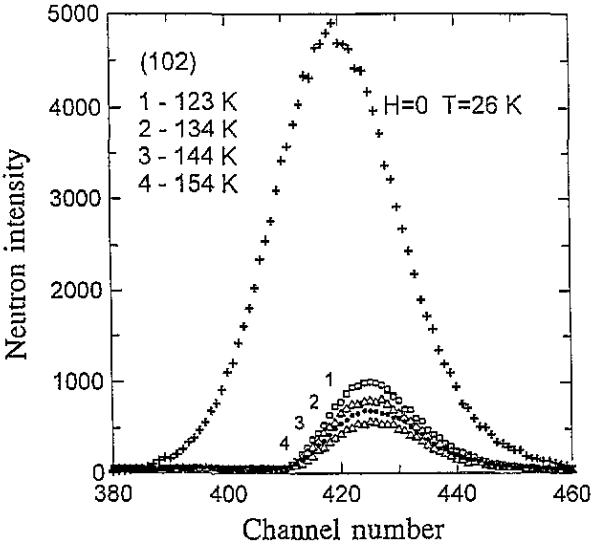

Figure 4. The correspondence between the diffraction peak (102) induced by a pulsed magnetic field with $H_m = 87.55$ kOe at the given temperatures, and the 'standard' peak ($H = 0$) measured at $T = 26$ K, $\tau = 16\,\mu$s.

Figure 3 shows a set of neutron patterns of (102) reflection obtained at different temperatures for a pulse amplitude $H_m = 77.0$ kOe and scattering angle $2\theta = 91.7°$. The treatment of these and similar data requires normalization of the neutron patterns against the 'standard' shape of the diffraction peak measured at low temperatures without an applied field. This is illustrated by figure 4, where the diffraction profiles of (102) reflection at $2\theta = 91.7°$ and $H_m = 87.55$ kOe are presented in combination with the (102) peak profile measured at $T = 26$ K, i.e. in the Γ_2 state where the sufficiently high-in-magnitude components C_y and c_y associated with (102) reflection are present. The normalization in this case consists of dividing the spectrum recorded in an applied field by the standard peak profile and multiplying the result by the standard peak area. This is done, of course, after subtraction of the background. The crystal reflectivity obtained in this way does not depend on the actual magnitude of the scattering amplitude of the standard peak, since in

the present case the latter characterizes just the time dependence of arrival of the neutrons of a given wavelength which participate in scattering.

It was taken into account that for small values of the induced components the kinematic approximation is fulfilled, i.e. the scattering intensity is proportional to the square of the scattering amplitude. We use here for the scattering amplitude the corresponding quantity related to one pair of iron and holmium ions and expressed in terms of spin units. Accordingly, for the two considered lattice planes, the scattering amplitude is

$$\begin{aligned} F_{(102)} &= f_{\mathrm{Fe}(102)} S_{\mathrm{Fe},x} + f_{\mathrm{Ho}(102)} \cos(2\pi\delta x) S_{\mathrm{Ho},x} \\ F_{(201)} &= f_{\mathrm{Ho}(201)} \sin(4\pi\delta x) S_{\mathrm{Ho},x} \end{aligned} \tag{4}$$

where f_{Fe} and f_{Ho} are the magnetic form factors corresponding to the given reflection, $S_{\mathrm{Fe},x}$ and $S_{\mathrm{Ho},x}$ are the effective spin components induced along the x axis and $\delta x = 0.018$ is the displacement of holmium from the unit cell edge along the x axis.

For the scattered diffraction intensity corresponding to a field amplitude H we have

$$I_H = \frac{I_0}{S_0} i(\lambda) 8 d_{hkl}^4 \sin^2\theta_0 N^2 V \cos^2\eta \, 4 \times 0.539 \times 10^{-12} |F_{hkl}|^2 \tag{5}$$

where I_0 is the intensity in the time channel of the 'standard' peak corresponding to the value H, S_0 is the area of the 'standard' peak, d_{hkl} is the interplanar distance, V is the sample volume and η is the angle between the x axis and the scattering plane.

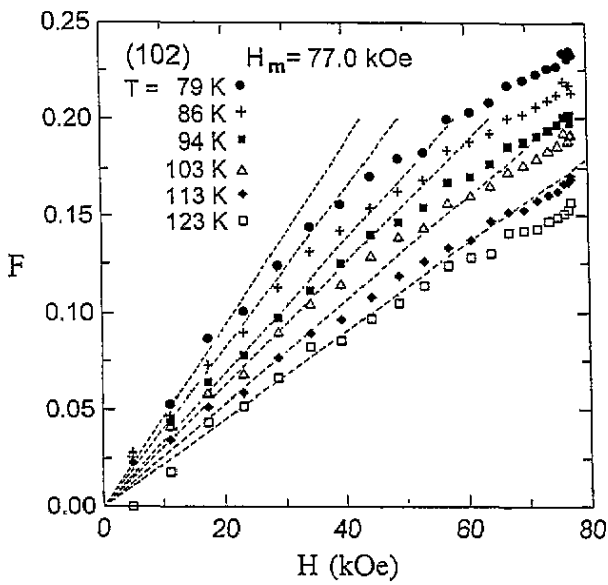

Figure 5. Variation of the scattering amplitude of (102) reflection with magnetic field. The amplitude of the pulsed magnetic field is $H_m = 77.0$ kOe.

Figures 5 and 6 display the results for (102) reflection from the treatment of the spectra shown in figures 3 and 4 according to (1) and (5). It is seen that there is a linear part of the dependence $F = f(H)$. The deviation from the linear dependence is connected with the violation of the quadratic dependence of the scattering intensity on the scattering amplitude due to neutron extinction within the single crystal.

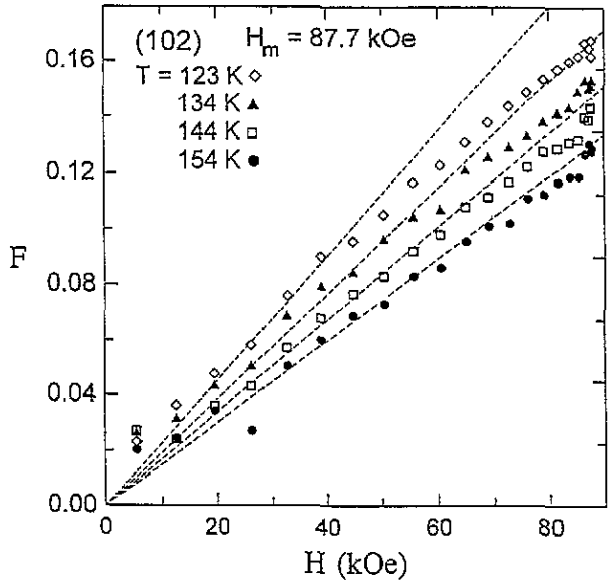

Figure 6. The scattering amplitude of (102) reflection as a function of magnetic field. The amplitude of the pulsed magnetic field is $H_m = 87.7$ kOe.

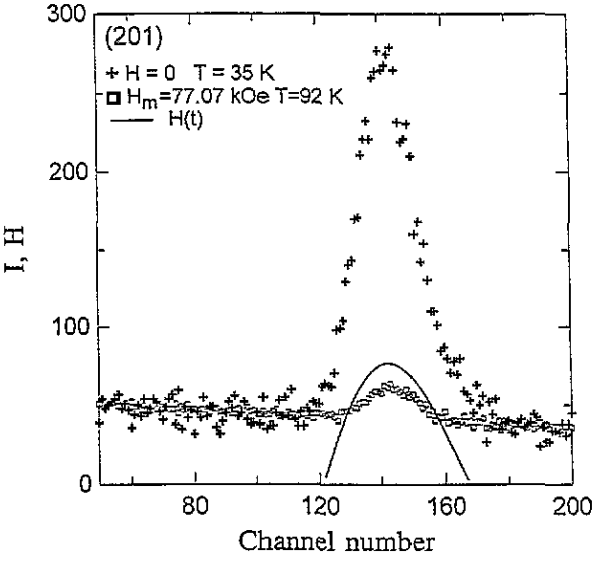

Figure 7. Profile intensity of (201) reflection at 35 K, induced diffraction peak (201) at 92 K and the shape of the applied magnetic pulse are presented on the same scale, against channel number, $\tau = 16\,\mu s$.

The neutron pattern of (201) reflection obtained at $H_m = 77.1$ kOe, $\tau = 16\,\mu$s, $T = 92$ K, $2\theta = 90°$ is shown in figure 7. The corresponding standard peak and magnetic field pulse are given as well.

The scattering amplitudes of (102) and (201) reflections obtained at the relatively close temperatures of 94 K and 92 K, respectively, are plotted in figure 8. Because of the rather large spread of the $F(201)$ data points, corresponding to small pulse amplitudes, they are not presented here. The data were treated using the following values of the form factors [11, 12]: $f_{Fe(102)} = 0.715$, $f_{Ho(102)} = 0.866$, $f_{Ho(201)} = 0.79$. By neglecting the differences in the scattering amplitudes at $T = 92$ K and $T = 94$ K we get at an average temperature $T = 93$ K the antiferromagnetic susceptibilities of iron and holmium

ions: $S_{Fe,x}/H_y = -2.02 \times 10^{-6}\,Oe^{-1}$ and $S_{Ho,x}/H_y = 5.58 \times 10^{-6}\,Oe^{-1}$. The sign of the respective susceptibility values corresponds to the change in sublattice magnetizations, illustrated in figure 1 by the arrows.

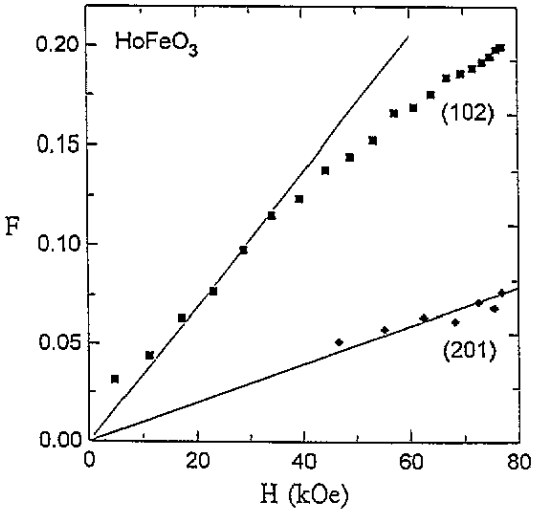

Figure 8. Magnetic field dependence of the scattering amplitudes of induced (102) reflection (at 94 K) and induced (201) reflection (at 92 K). The straight lines pass through the origin as observed in the absence of an external magnetic field.

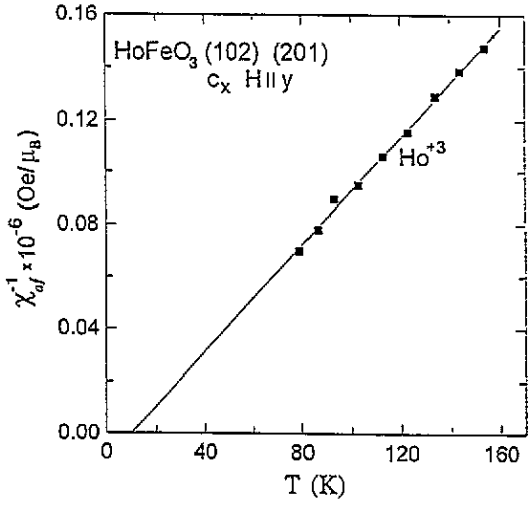

Figure 9. Temperature dependence of the antiferromagnetic susceptibility of Ho^{3+} ions.

With the aim of extracting the antiferromagnetic susceptibility of the holmium subsystem we neglect the temperature dependence of the iron sublattices in the range of temperatures under consideration. This we find acceptable, since the applied field is perpendicular to the vector G of the main antiferromagnetism of Fe ions and the sublattice magnetizations are near saturation. Therefore, the magnitude of the induced weak antiferromagnetism of C type for iron ions cannot depend significantly on temperature.

In this approximation, i.e. using the value $S_{Ho,x}/H_y = 5.58 \times 10^{-6}\,Oe^{-1}$ at all temperatures, by means of equation (4) we extract from figures 5 and 6 the temperature

dependence of the antiferromagnetic susceptibility of Ho ions, plotted in figure 9, and it is clearly seen that it obeys the Curie–Weiss law

$$\chi_{af} \equiv 2\frac{S_{Ho,x}}{H_y} = \frac{0.975 \times 10^{-3}}{T - 9.6}\frac{\mu_B}{Oe} \tag{6}$$

with a positive constant $\Theta = 9.6$ K.

This compliance with the Curie–Weiss law occurs as a consequence of the paramagnetic state of Ho^{3+} ions. A positive sign of the Curie–Weiss constant Θ should not give grounds for surprise because, in contrast to the ordinary magnetic susceptibility, the antiferromagnetic susceptibility used in the present study, in the case of asymptotic extrapolation to the low-temperatures region, should diverge just at the characteristic Néel temperature of the rare-earth subsystem, which corresponds to antiferromagnetic ordering of type **c**.

One should not expect coincidence of the value of Θ obtained with the known values of the Néel point for the Ho^{3+} subsystem (4.55 K [1], 6.5 K [2]) because the cited values are related to the low-temperature spin configuration Γ_2, for which the interactions responsible for the antiferromagnetic ordering of the Ho subsystem are somewhat different from the state Γ_4. In addition, the authors of the present study do not claim a high accuracy of the value of Θ obtained in view of the difficulties encountered, in particular in determining the linear portions of the curves presented in figures 5 and 6. Also, in extrapolating to the low-temperature region, one should take into account the thermal expansion of the crystal, something which has not been done in this work.

Acknowledgments

The partial financial support of the Ministry of Education and Science of Bulgaria under a contract with the National Fund for Science is gratefully acknowledged.

References

[1] Grambow I, Kronauer P, Schneider J and Shuchert M 1967 *Z. Natur.* A **22** 828
[2] Mareshal J and Sivardiere J 1969 *J. Physique* **30** 967.
[3] Bertaut E F 1963 *Magnetism III* ed G Rado and H Suhl (New York: Academic)
[4] Gorodetsky G and Treves D 1964 *Phys. Rev.* A **135** 97
[5] Yamaguchi T 1974 *J. Phys. Chem. Sol.* **35** 479
[6] Ananiev B *et al* 1989 *JINR Commun.* P13-89-517, Dubna
[7] Varenik G *et al* 1989 *JINR Commun.* P13-89-518, Dubna
[8] Nietz V V 1970 *JINR Commun.* P3-5372, Dubna
[9] Georgiev D, Krezhov K and Nietz V V 1995 *Solid State Commun.* to appear
[10] Plakhtii V, Chernenkov Yu, Schweizer J and Bedrizova M 1981 *Zh. Eksp. Theo. Fiz.* **80** 2465
[11] Nathans R, Pickart S and Alperin H 1960 *Bull. Amer Soc.* **5** 455
[12] Bertaut E F *et al* 1964 *Proc. Int. Conf. Magnetism, Nottingham* p 275